Cross sections for electron scattering by formaldehyde and pyrimidine in the low- and intermediate-energy ranges

J. R. Ferraz,[1] A. S. dos Santos,[1] G. L. C. de Souza,[2] A. I. Zanelato,[2] T. R. M. Alves,[2] M.-T. Lee,[3] L. M. Brescansin,[4] R. R. Lucchese,[5] and L. E. Machado[1]

[1]*Departamento de Física, UFSCar, 13565-905 São Carlos, São Paulo, Brazil*
[2]*Instituto de Ciências Exatas e Tecnologia, UFAM, 69100-000 Itacoatiara, Amazonas, Brazil*
[3]*Departamento de Química, UFSCar, 13565-905 São Carlos, São Paulo, Brazil*
[4]*Instituto de Física "Gleb Wataghin", UNICAMP, 13083-970 Campinas, São Paulo, Brazil*
[5]*Department of Chemistry, Texas A & M University, College Station, Texas 7784-3255, USA*

(Received 19 December 2012; published 25 March 2013)

We report a theoretical study on electron scattering by two strongly polar molecules, namely, formaldehyde (CH_2O) and pyrimidine ($C_4H_4N_2$), in the low- and intermediate-energy ranges. Calculated elastic differential, integral, and momentum-transfer cross sections, as well as total (elastic + inelastic) and total absorption cross sections, are reported for impact energies ranging from 0.2 to 500 eV. A complex optical potential is used to represent the electron-molecule interaction dynamics, whereas a single-center-expansion method associated with the Padé approximant technique is used to solve the scattering equations. Our calculated results are compared with experimental results and other theoretical data available in the literature. Generally good agreement is seen in these comparisons.

DOI: 10.1103/PhysRevA.87.032717 PACS number(s): 34.80.Bm

I. INTRODUCTION

Recently, electron scattering from small organic molecules has been a subject of increasing interest, both theoretically and experimentally. The interest in such studies resides mainly in many applications of these species. For instance, cross sections of electron scattering by those molecules are important for understanding and modeling plasmas [1], to elucidate some mechanisms of astrophysical phenomena [2], and to control plasma processing in industry [3]. In particular, alcohols and biodiesels are currently used as renewable energy sources replacing the traditional fossil fuels. Such uses could lead to the increase of vapor concentration of these fuels in the atmosphere in the near future. Therefore, the investigation of electron interaction with them may help in the understanding of energy and material balances in combustion plasmas, as well as in the understanding of their chemistry in terrestrial atmosphere.

Moreover, radiation damage in biomolecular systems has been the subject of extensive research in the past few years. This interest is mainly due to the fact that significant damage can be caused in DNA via interaction with low-energy electrons, leading either to direct single- and double-strand breaks [4] or to the formation of free radicals, which can then chemically react with DNA, also leading to strand breaks. Ionizing radiation is widely used in medicine as a probe in radiodiagnostic examinations and as a genotoxic agent in radiotherapy. The major part of the energy deposited by ionizing radiation in condensed matter can lead to the production of abundant secondary electrons. In order to better understand the physical and chemical processes responsible for DNA damage, absolute-cross-section data of electron impact on DNA and its constituents are needed.

Many molecules of interest such as alcohols, biodiesels, and the constituents of the bases and backbone of DNA are strongly polar, which makes the measurement of their differential cross sections (DCS) at small scattering angles highly unreliable. In this sense, the development of theoretical methods is important in order to amend this problem. With this motivation in mind, in this work we present a theoretical investigation of electron scattering by two highly polar molecules, namely, formaldehyde (CH_2O) and pyrimidine ($C_4H_4N_2$), in a wide incident energy range.

Probably because formaldehyde is one of the simplest polar organic molecules, the first investigations of e^--CH_2O collisions were performed back in the 1970s. For instance, earlier electronic spectroscopic studies on CH_2O include those by Weiss *et al.* [5] and Chutjian [6]. Both studies used the crossed-beam technique and several electronic transitions in this compound were observed. Using the electron-transmission technique, Burrow and Michejda [7] observed pronounced Feshbach resonances at energies above 6 eV in their relative total cross sections (TCS). These authors also reported the occurrence of resonances in the 0.5–3.0 eV impact energy range. Lately, Benoit and Abouaf [8] reported vibrational excitations in e^--CH_2O collisions in the 0.4–2.6 eV energy range. These authors have confirmed the existence of a strong shape resonance at around 1 eV. Also, Van Veen *et al.* [9] measured the excitation function for the ($n \rightarrow \pi^*$) transition by using the trapped-electron method. Nevertheless, to our knowledge, there are no absolute-cross-section measurements for e^--CH_2O scattering reported in the literature.

On the theoretical side, both elastic and inelastic e^--CH_2O collisions in the low-energy range were investigated by Rescigno *et al.* [10,11] and Schneider *et al.* [12] using the complex Kohn variational method. In their work, Rescigno *et al.* [10] identified a $^2B_1$ shape resonance at about the same energy region previously observed by Benoit and Abouaf [8]. This resonance was also studied by Mahalakshmi and Mishra [13] using the propagator technique. In 2001, Sobrinho *et al.* [14] reported DCS and momentum-transfer cross sections (MTCS) for elastic scattering, as well as for the two lowest electronic transitions in formaldehyde in the 16–80 eV energy range by using the iterative Schwinger variational method (ISVM). Kaur and Baluja [15] reported

DCS, MTCS, and integral cross sections (ICS) for e^--CH_2O collisions in an eight-state multichannel calculation using the R-matrix method in the 0.1–20 eV range. Freitas *et al.* [16] also reported DCS and MTCS for elastic electron scattering by both formaldehyde and the binary CH_20-H_2O complex at several different geometries using the Schwinger multichannel method (SMC). More recently, TCS for e^--CH_2O scattering were calculated by Zecca *et al.* [17] using the independent atom model–screened additivity rule (IAM-SCAR) method for incident energies varying from 1 to 10 000 eV. In the same paper, DCS and MTCS for elastic e^+-CH_2O collisions calculated using the SMC were also reported. Also very recently, TCS for e^--CH_2O scattering in the 0.01–2000 eV energy range were calculated by Vinodkumar *et al.* [18] using a combination of the R-matrix method and the spherical complex optical potential (SCOP) method.

In contrast to formaldehyde, only recently have investigations on electron-pyrimidine collisions started appearing in the literature. This interest derives mainly from the possible radiation damage of DNA. Pyrimidine is a heterocyclic, aromatic organic compound containing two nitrogen atoms at positions 1 and 3 of the six-member ring. Due to the similarity of its ring structure to three of the five nucleobases, namely, cytosine ($C_4H_5N_3O$), thymine ($C_5H_6N_2O_2$), and uracil ($C_4H_4N_2O_2$), it is considered a model molecule for studies of electron interactions with DNA and RNA bases. Recently, e^--$C_4H_4N_2$ collisions have been intensively investigated both theoretically and experimentally. For instance, DCS and ICS for elastic scattering by pyrimidine were measured by Palihawadana *et al.* [19] in the 3–50 eV energy range and also by Maljković *et al.* [20] in the 50–300 eV range. Vibrational and electronic excitation cross sections for electron impact on condensed pyrimidine were determined by Levesque *et al.* [21]. DCS and ICS for low-energy electron-impact excitation of the unresolved combinations of the $2\,^3B_2 + 2\,^1A_1$ and $3\,^1A_1 + 2\,^1B_2$ electronic states of pyrimidine were reported by Jones *et al.* [22] at 15 and 30 eV incident energies. ICS for inelastic e^--$C_4H_4N_2$ collisions were recently measured by Mašín *et al.* [23] in the 15–50 eV range.

Theoretically, DCS and ICS for elastic e^--$C_4H_4N_2$ collisions were calculated by Palihawadana *et al.* [19] in the 0.1–50 eV energy range using both the SMC and IAM-SCAR methods. In their SMC ICS, calculated without including dipole correction, three strong resonances were identified. The peaks located at 0.38 and 4.6 eV are due to shape resonances occurring in $^2B_1$ symmetry, while the peak located at 0.63 eV is associated with a resonance of $^2A_2$ symmetry. Also, DCS and ICS up to 15 eV were calculated by Mašín *et al.* [23] using the R-matrix method. Two theoretical frameworks, namely, the static-exchange-polarization (SEP) and the close-coupling (CC) approximations, were used in their calculations. Resonances similar to those of Palihawadana *et al.* [19] were also seen in their calculated ICS. In their SEP model, these resonances were located at 0.21 eV for $^2A_2$ symmetry and at 0.68 and 5.15 eV for $^2B_1$ symmetry. Moreover, the IAM-SCAR method was also used by Maljković *et al.* [20] to calculate DCS and ICS in the 50–300 eV range and by Zecca *et al.* [24] to calculated TCS in the 1–10 000 eV range.

At energies above the ionization threshold, a number of inelastic scattering channels such as electronic excitation and ionization of the target are open, leading to a reduction in the electronic flux of the elastic scattering channel. Such effects (known as absorption effects) are difficult to account for in scattering calculations in an *ab initio* approach. Therefore, several semiempirical model absorption potentials have been proposed and applied within the single-channel framework [25,26]. Among them, the scaled quasi-free-scattering model (SQFSM), which is an improvement of the quasi-free-scattering model version 3 (QFSM3) of Staszewska *et al.* [27], was proposed by our group a few years ago [28,29]. In general, DCS, ICS, and MTCS calculated using the SQFSM for elastic electron-molecule scattering do not differ significantly from those computed using the QFSM3. However, for a variety of atomic and molecular targets [29–31], the agreement between the TCS and total absorption cross sections (TACS) calculated with the SQFSM and the corresponding experimental data is significantly better than the agreement with their QFSM3 counterparts. This improvement was confirmed by a recent benchmark study of Staszewska *et al.* [32] for electron-atom collisions. In the present work, the SQFSM absorption potential, combined with the static-exchange-correlation-polarization contribution, is applied to describe the dynamics of electron collisions with formaldehyde and pyrimidine. Particularly, for incident energies above 50 eV, the introduction of absorption effects in the collision dynamics should significantly reduce the magnitude of the DCS at intermediate and large scattering angles.

The organization of this paper is as follows: In Sec. II, the theory is briefly described. In Sec. III, some details of the calculations for each target are presented and our calculated results are compared with the experimental data available in the literature, as well as with other existing theoretical data. A brief conclusion is also summarized in this section.

II. THEORY

In the present study, a complex optical potential given by

$$V_{\rm opt} = V_{\rm st} + V_{\rm ex} + V_{\rm cp} + i\,V_{\rm ab} \tag{1}$$

is used to represent the e^--molecule interaction dynamics. In the above equation, $V_{\rm st}$ and $V_{\rm ex}$ are the static and the exchange components, respectively; $V_{\rm cp}$ is the correlation-polarization contribution; and $V_{\rm ab}$ is an absorption potential. Using this potential, the scattering problem is solved using the numerical solution of the Lippmann-Schwinger (LS) integral equation within the single-center-expansion close-coupling framework and further corrected using the Padé approximant technique. The basic theory of this method has already been presented elsewhere [31] and is only briefly outlined here.

The procedure starts by using the two-potential formalism to write the reduced complex optical potential $U_{\rm opt} = 2V_{\rm opt}$ as a sum:

$$U_{\rm opt} = U_1 + U_2, \tag{2}$$

where

$$U_1 = U_{\rm st} + U_{\rm ex}^{\rm loc} + U_{\rm cp} \tag{3}$$

and

$$U_2 = U_{\rm ex} - U_{\rm ex}^{\rm loc} + i\,U_{\rm ab}. \tag{4}$$

In the present work, U_{st} and U_{ex} are derived exactly from a near-Hartree-Fock self-consistent-field (SCF) target wave function, whereas U_{cp} is obtained in the framework of the free-electron-gas model, derived from a parameter-free local density, as prescribed by Padial and Norcross [33]. The Hara free-electron-gas-exchange potential [34] is used to generate the local-exchange potential U_{ex}^{loc}. U_{ab} is the reduced SQFSM absorption potential of Lee *et al*. [28].

The T matrix can then be written as

$$T_{fi} = T_1 + T_2, \tag{5}$$

where

$$T_1 = \langle \chi(\vec{k}_f)|U_1|\psi_1^+(\vec{k}_i)\rangle \tag{6}$$

and

$$T_2 = \langle \psi_1^-(\vec{k}_f)|U_2|\psi^+(\vec{k}_i)\rangle. \tag{7}$$

In Eq. (6), χ is the unperturbed plane wave function and ψ_1 is the numerical solution of the Schrödinger equation for the U_1 potential:

$$(\nabla^2 + k^2 - U_1)\psi_1^{\pm}(\vec{r}) = 0. \tag{8}$$

Next, T_2 is evaluated by using the Padé approximant technique in an iterative procedure similar to that developed by Lucchese and McKoy [35] for linear molecules. The $[N/N]$ Padé approximant for T_2 is given as [36]

$$T_2[N/N] = -\sum_{i,j=1,N-1} \langle \psi_1^-|U_2|\phi^{(i)+}\rangle (D^{-1})_{ij} \langle \phi^{(j)-}|U_2|\psi_1^+\rangle, \tag{9}$$

where

$$D_{ij} = \langle \phi^{(i)-}|U_2 - U_2 G_1^+ U_2|\phi^{(j)+}\rangle \tag{10}$$

and ϕ is given as

$$\phi^{(i)\pm} = (G_1^{\pm}U_2)^i \psi_1^{\pm}, \tag{11}$$

where $\phi^{(0)} = \psi_1$ and $G_1^{\pm}$ is a distorted-wave Green's function which satisfies the following condition:

$$(\nabla^2 + k^2 - U_1)G_1^{\pm}(\vec{r},\vec{r}') = \delta(\vec{r},\vec{r}'). \tag{12}$$

The superscripts $-$ and $+$ in the above equations denote the incoming- and outgoing-boundary conditions of the scattering waves, respectively. In our calculations, both the scattering wave function and the interaction potential are single-center expanded in terms of the symmetry-adapted functions [37] as has been done, for example, in Ref. [31].

It is known that for targets with considerable permanent dipole moments, partial-wave expansions converge slowly due to the long-range nature of the dipole interaction potential. In order to overcome this difficulty, a Born-closure formula is used to account for the contribution of higher partial-wave components to the scattering amplitudes. The procedure used is the same as that used in some of our previous studies [38–40].

Briefly, the vibronically elastic DCS is calculated within the adiabatic-nuclei-rotation framework:

$$\frac{d\sigma}{d\Omega} = \sum_{J'\tau'} \frac{d\sigma}{d\Omega}(J = 0, \tau = 0 \longrightarrow J'\tau'), \tag{13}$$

where

$$\frac{d\sigma}{d\Omega}(J\tau \longrightarrow J'\tau') = \frac{1}{(2J+1)}\frac{k}{k_0}\sum_{M=-J}^{J}\sum_{M'=-J'}^{J'} \times |f_{J\tau M \longrightarrow J'\tau' M'}|^2 \tag{14}$$

and

$$f_{J\tau M \longrightarrow J'\tau' M'} = \langle \Psi_{J'\tau' M'}(\Omega) \mid f^{LF} \mid \Psi_{J\tau M}(\Omega)\rangle. \tag{15}$$

In the above equation, $\Psi_{J\tau M}(\Omega)$ are eigenfunctions of an asymmetric-top rotor and f^{LF} is the electronic part of the laboratory-frame (LF) scattering amplitude which can be related to the corresponding body-frame (BF) T matrix by an usual frame transformation [41]. The Born-closure-corrected T matrix which accounts for the contribution of higher partial-wave components to the scattering amplitude is written as

$$T = T^B + \frac{1}{k}\sum_{p\mu lhl'h'}^{LL'} i^{l-l'}\left(T^{p\mu}_{k,lh;l'h'} - T^{p\mu^B}_{k,lh;l'h'}\right) \times X^{p\mu}_{lh}(\hat{k}) X^{p\mu^*}_{l'h'}(\hat{k}_0), \tag{16}$$

where $X^{p\mu}_{lh}(\hat{k})$ are the symmetry-adapted functions [37] which are expanded in terms of the usual spherical harmonics as follows,

$$X^{p\mu}_{lh}(\hat{r}) = \sum_m b^{p\mu}_{lhm} Y_{lm}(\hat{r}), \tag{17}$$

and T^B is the complete point-dipole first-Born-approximation (FBA) T matrix, $T^{p\mu}_{k,lh;l'h'}$ are the partial-wave T-matrix elements calculated via the Padé approximant technique, and $T^{p\mu^B}_{k,lh;l'h'}$ are the corresponding partial-wave point-dipole FBA T-matrix elements, given by

$$T^{p\mu^B}_{k,lh;l'h'} = -\frac{D}{L}\left[\frac{(L+h)(L-h)}{(2L+1)(2L-1)}\right]^{\frac{1}{2}}, \tag{18}$$

where D is the target electric dipole moment and $L = l'$ when $l' = l + 1$ and $L = l$ when $l' = l - 1$.

Moreover, the TCS for electron-molecule scattering are obtained using the optical theorem:

$$\sigma_{tot} = \frac{4\pi}{k}\mathrm{Im}[f(\theta = 0^\circ)]. \tag{19}$$

III. COMPUTATIONAL DETAILS AND RESULTS

A. Formaldehyde

The Hartree-Fock (HF) SCF wave function for ground-state formaldehyde was obtained using the standard contracted Gaussian functions of Dunning [42], specifically, a $[9s5p/5s3p]$ basis set augmented by three s (α = 0.0473, 0.0125, and 0.0045), four p (α = 0.0825, 0.365, 0.125, and 0.0035), and three d (α = 0.756, 0.15, and 0.0375) uncontracted functions for the carbon center; a $[9s5p/3s3p]$ basis set augmented by three s (α = 0.05, 0.02, and 0.005), one p (α = 0.04), and three d (α = 1.7, 0.85, and 0.34) uncontracted functions for the oxygen center; and a $[4s4p/2s1p]$ basis set augmented by three p (α = 0.3, 0.012, and 0.04) uncontracted functions for the hydrogen centers. At the experimental equilibrium geometry of $R_{(O\text{-}C)} = 2.286$ a.u. and

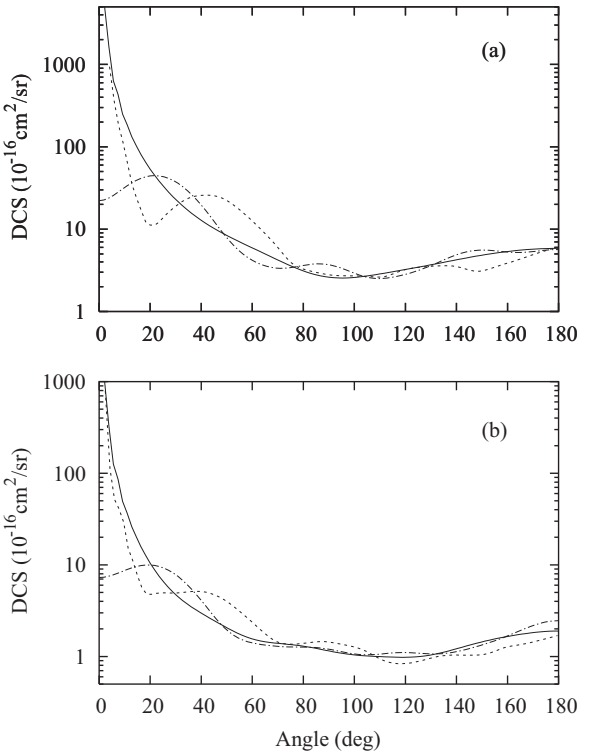

FIG. 1. DCS for elastic e^--CH_2O scattering at (a) 1 eV and (b) 5 eV. Solid line, present results calculated with the Born-dipole correction; dotted-dashed line, present results calculated without the Born-dipole correction; short-dashed line, calculated R-matrix data of Kaur and Baluja [15].

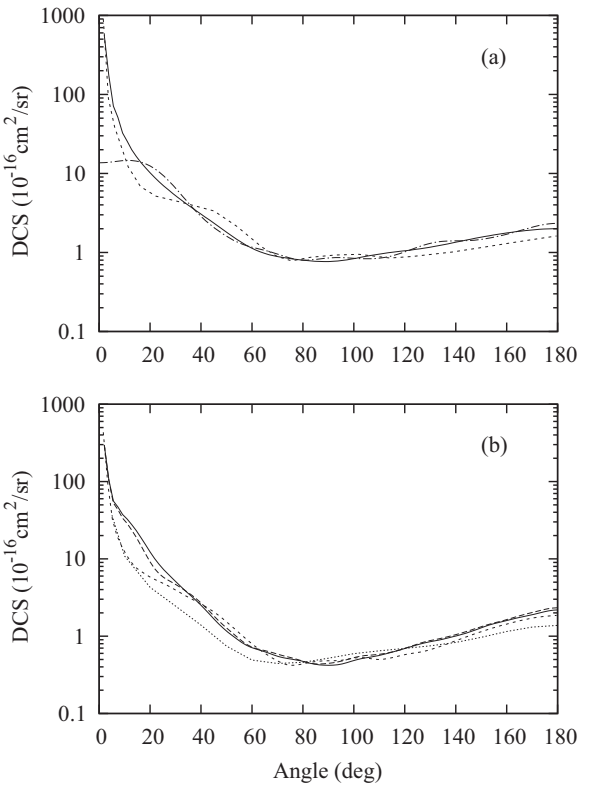

FIG. 2. DCS for elastic e^--CH_2O scattering at (a) 10 eV and (b) 20 eV. Symbols are the same as those in Fig. 1 with the addition of the following: dashed-line, present Born-corrected DCS calculated without inclusion of absorption effects; dotted line, calculated ISVM data of Sobrinho *et al.* [14].

$R_{(C\text{-}H)} = 2.082$ a.u. this basis set gives an SCF energy of $-113.910\ 11$ a.u. and a permanent dipole moment of 2.85 D, in reasonable agreement with the experimental value of 2.34 D [43]. The calculated dipole polarizabilities $\alpha_{xx} = 16.2486$ a.u., $\alpha_{yy} = 12.3328$ a.u., and $\alpha_{zz} = 21.0777$ a.u. were used to obtain the asymptotic form of V_{cp}. For incident energies of 15 eV and below, the absorption effects are negligible and therefore are not taken into account in the calculations.

In our study, all the single-center expansions were truncated at $l_c = 8$, 18, and 25 at incident energies lower than 15 eV, between 15 and 100 eV, and above 100 eV, respectively. All calculated cross sections were converged within five iterations.

In Figs. 1–4 we show our theoretical DCS, calculated with the Born-dipole correction, for elastic e^--CH_2O scattering in the 1–300 eV energy range, and also those calculated without the Born-dipole correction at 1, 5, and 10 eV. The theoretical results of Kaur and Baluja [15] obtained using the R-matrix method and those of Sobrinho *et al.* [14] using the ISVM [44], are shown at energies for which comparisons are possible. Unfortunately, to our knowledge, no experimental results for this target are available in the literature.

In Figs. 1 and 2, our DCS calculated without the Born correction show some oscillations, specially at 1 and 5 eV. They also present a falloff behavior at scattering angles near the forward direction, which is unphysical for polar targets. On the other hand, the DCS calculated with Born corrections are much smoother and are also forwardly peaked, as expected. Although the Born-corrected R-matrix DCS of Kaur and

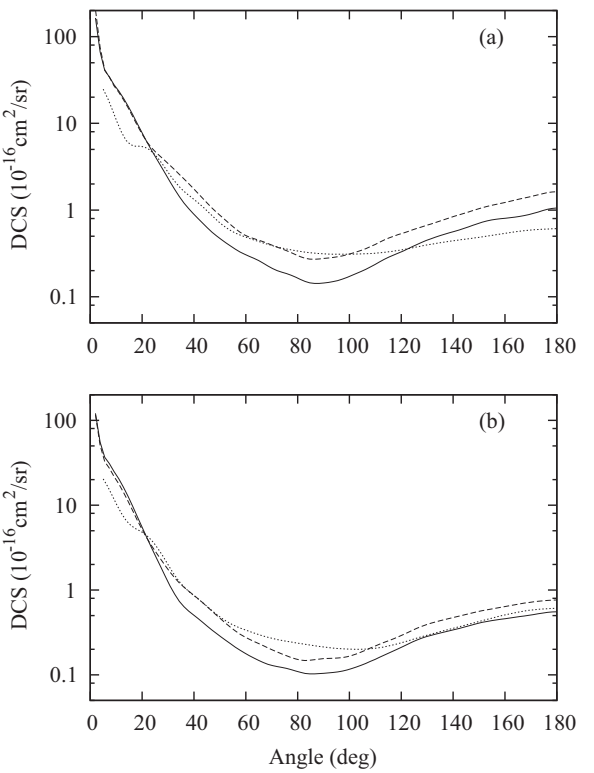

FIG. 3. DCS for elastic e^--CH_2O scattering at (a) 40 eV and (b) 60 eV. Symbols are the same as those in Fig. 2.

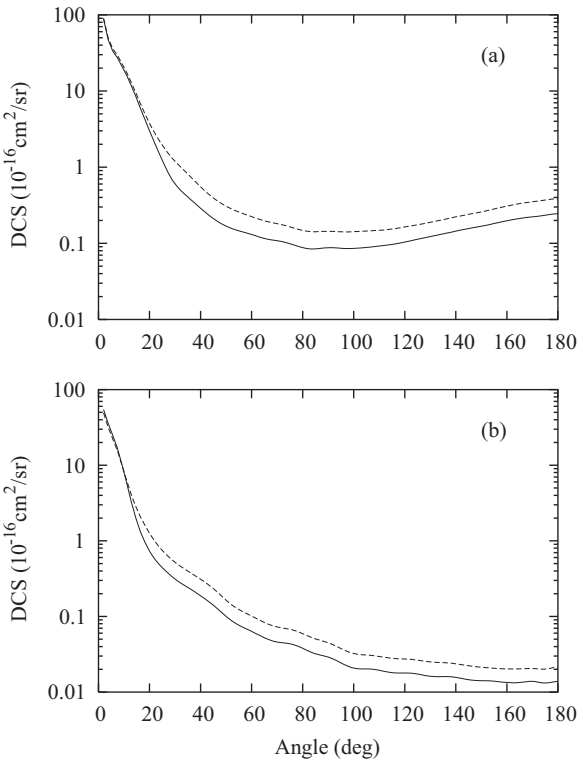

FIG. 4. DCS for elastic e^--CH_2O scattering at (a) 100 eV and (b) 300 eV. Symbols are the same as those in Fig. 2.

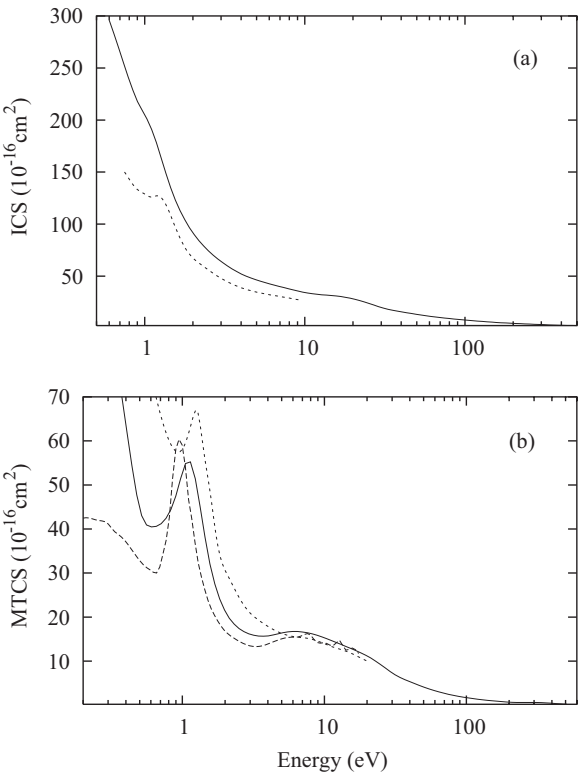

FIG. 5. (a) ICS and (b) MTCS for elastic e^--CH_2O scattering. Solid line, present theoretical results calculated with the Born-dipole correction; short-dashed line, calculated R-matrix data of Kaur and Baluja [15]; dashed line, SMC results of Freitas *et al.* [16].

Baluja [15] present the correct forward-direction behavior, some oscillations are still seen in their results. These observed oscillations may be due to the fact that the dipole-Born correction made by them was not on the scattering amplitudes but directly on the cross sections, which is given as

$$\frac{d\sigma}{d\Omega} = \frac{d\sigma^B}{d\Omega} + \sum_L \left(A_L - A_L^B\right) P_L(\cos\theta). \qquad (20)$$

Using this approximation, interference terms between the low-L and high-L partial-wave components are omitted.

At 20 eV, the ISVM DCS of Sobrinho *et al.* [14] calculated at the SEP level of approximation and our calculated data without accounting for absorption effects are also shown. A reasonable agreement among all the theoretical data is seen and also that the absorption effects are still not relevant at this energy.

In Figs. 3 and 4 we compare our DCS, calculated with and without the inclusion of absorption effects, in the 40–300 eV energy range. At 40 and 60 eV the results of Sobrinho *et al.* [14] obtained using the ISVM at the SEP approximation level are also included for comparison. For all energies in this range, the influence of the inelastic scattering channels on elastic collisions is evident: the DCS calculated including absorption effects lie well below those calculated without including them; the loss of electron flux in the elastic channel is a consequence of the open inelastic channels. The SEP data of Sobrinho *et al.* [14] agree with our results calculated without including absorption effects in the intermediate angular range.

In Figs. 5(a) and 5(b) we show our calculated ICS and MTCS, respectively, for elastic e^--CH_2O scattering in the 0.2–500 eV energy range, along with those of Kaur and Baluja [15] calculated using the R-matrix method and the SMC MTCS of Freitas *et al.* [16] calculated at the C_{2v} group and at the SEP level of approximation. Again, our calculated data for energies of 20 eV and above include absorption effects. Both our ICS and MTCS exhibit a resonancelike feature at around 1 eV. This feature is better characterized in the MTCS and is identified as a shape resonance in the B_1 partial scattering channel. This resonance was also identified by Kaur and Baluja [15] and by Freitas *et al.* [16], but was slightly shifted in energy. Although there are no experimental ICS and/or MTCS for this target to compare with calculations, experimental evidence of the existence of this resonance is given by Benoit and Abouaf [8] who observed the occurrence of a resonance near 1 eV in their measured energy-dependent fixed-angle (90°) vibrational excitation DCS, which is due to the occupation of the first empty $2b_1$ orbital by the scattering electron. The partial-channel ICS from our calculation have confirmed this assignment. Quantitatively, our ICS lie systematically above those of Kaur and Baluja [15] in the overlapped energy range. The difference between the two sets of ICS decreases with energy. In contrast, the MTCS calculated by Kaur and Baluja [15] are larger than ours at energies below 5 eV. On the other hand, our MTCS agree fairly well with the SMC data of Freitas *et al.* [16] at energies above 0.8 eV.

In Figs. 6(a) and 6(b) we present our TCS and TACS, respectively, calculated at incident energies up to 500 eV, along with the R-matrix TCS of Kaur and Baluja [15], the TCS of Zecca *et al.* [17] calculated using the IAM-SCAR, and the TCS of Vinodkumar *et al.* [18] calculated using the R-matrix

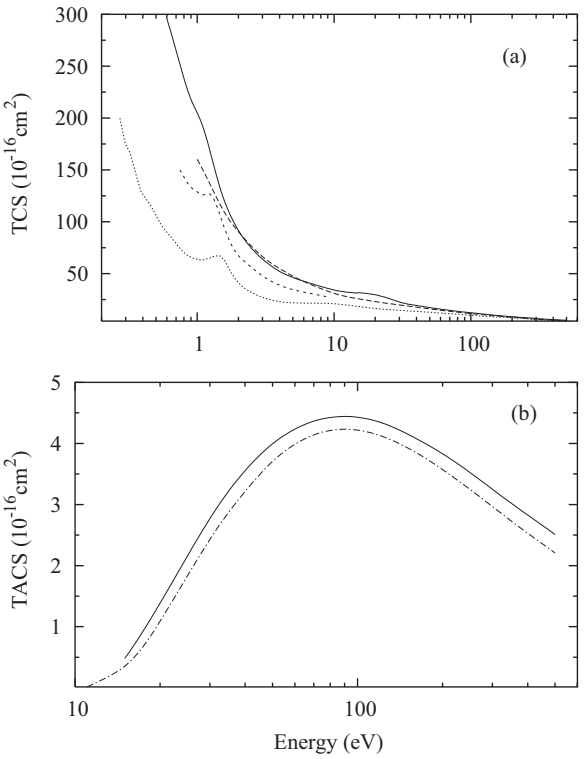

FIG. 6. (a) TCS and (b) TACS for e^--CH_2O scattering. Solid line, present theoretical results calculated including absorption effects; short-dashed line, calculated *R*-matrix data of Kaur and Baluja [15]; dashed line, calculated IAM-SCAR data of Zecca *et al.* [17]; dotted line, calculated SCOP data of Vinodkumar *et al.* [18]; dotted-dashed line, calculated BEB TICS of Kim and Irikura [45].

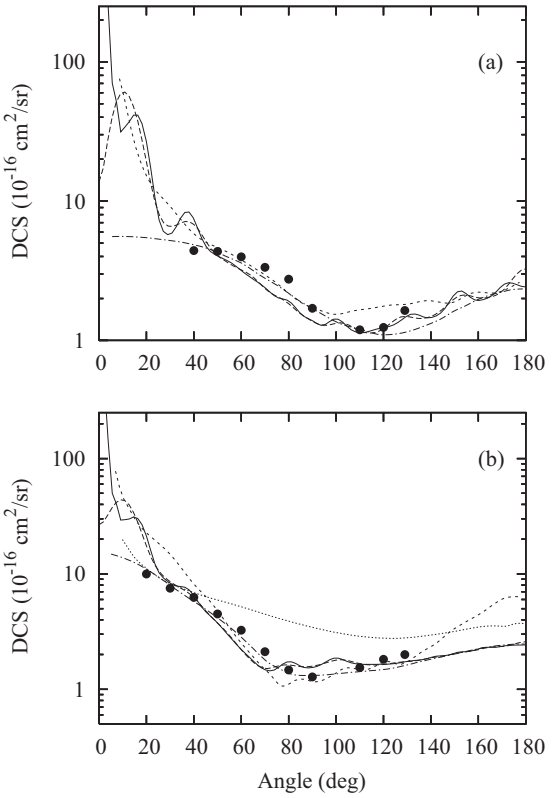

FIG. 7. DCS for elastic e^--$C_4H_4N_2$ scattering at (a) 3 eV and (b) 6 eV. Solid line, present results calculated with the Born-dipole correction; dashed line, present results calculated without the Born-dipole correction; short-dashed line, calculated *R*-matrix data of Mašín *et al.* [23]; dotted-dashed line, calculated SMC data of Palihawadana *et al.* [19]; dotted line, calculated IAM-SCAR data of Palihawadana *et al.* [19]; solid circles, experimental data of Palihawadana *et al.* [19].

approach for incident energies up to 20 eV and using the SCOP approximation above 20 eV. In Fig. 6(b) we compare our TACS with the total ionization cross sections (TICS) of Kim and Irikura [45], calculated using the binary-encounter Bethe (BEB) model. In general, all calculated TCS present similar qualitative energy-dependent behavior. However, the IAM-SCAR TCS of Zecca *et al.* [17] do not show the $^1B_1$ resonance feature at around 1 eV. In the entire energy range, the magnitudes of the TCS of Vinodkumar *et al.* [18] are significantly smaller than all other calculated results. The lack of the Born-type correction for the dipole interaction is probably the origin of this discrepancy. On the other hand, the IAM-SCAR data of Zecca *et al.* [17] are in good agreement with our calculated TCS at energies above 2 eV. In Fig. 6(b) one can notice a very good qualitative and quantitative agreement between our present TACS and the BEB TICS of Kim and Irikura [45]. The fact that their results are slightly below ours is expected since only ionization processes are taken into account in TICS calculations, whereas all inelastic processes are included in the SQFSM absorption potentials.

B. Pyrimidine

The SCF wave functions of the ground-state pyrimidine used in the generation of the e^--target potential were calculated at the HF SCF level. The calculations were performed using the quantum chemistry code GAMESS [46] with an Triple-Zeta Valence plus d-Polarization (TZVDP) contracted Gaussian basis set. The calculation was performed at the C_{2v} point group using the optimized equilibrium geometry taken from the literature [47]. The calculated SCF total energy is −262.767 36 a.u., slightly lower than the HF results of −262.75 a.u. calculated by Mašín *et al.* [23]. Our calculated permanent dipole moment is 2.385 D, in good agreement with the experimental value of 2.334 ± 0.01 D [48]. Moreover, the theoretical dipole polarizabilities $\alpha_{xx} = 22.54$ a.u., $\alpha_{yy} = 55.06$ a.u., and $\alpha_{zz} = 59.06$ a.u. were used for the generation of the asymptotic form of V_{cp}. These values, calculated within the HF framework using an aug-cc-pVDZ basis, were also taken from the database of the NIST website [47].

In the present study, the single-center expansions of bound and scattering wave functions, as well as the interaction potentials and all related matrices were truncated at $l_c = 25$ in the entire incident energy range covered herein. All the calculated cross sections were converged within seven iterations.

In Figs. 7 and 8 we show our theoretical DCS, calculated both with and without the Born-dipole correction, for elastic e^--$C_4H_4N_2$ scattering in the 3–15 eV range. As in formaldehyde, the absorption effects were neglected in this energy range. In addition, the experimental data of Palihawadana *et al.* [19], as well as the calculated DCS using both the SMC

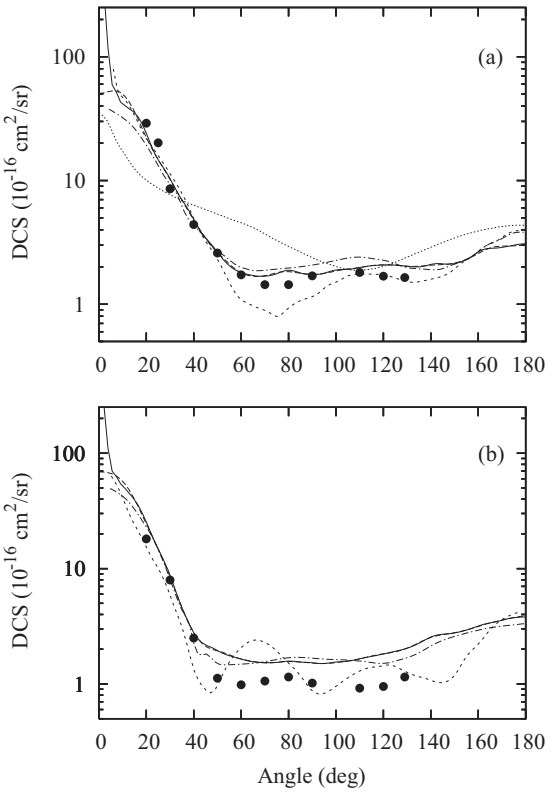

FIG. 8. DCS for elastic e^--$C_4H_4N_2$ scattering at (a) 10 eV and (b) 15 eV. Symbols are the same as those in Fig. 1.

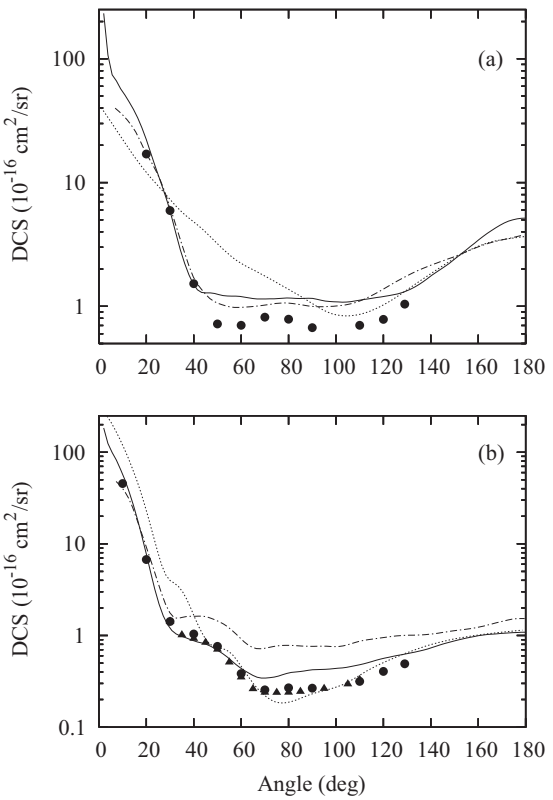

FIG. 9. DCS for elastic e^--$C_4H_4N_2$ scattering at (a) 20 eV and (b) 50 eV. Symbols are the same as those in Fig. 1 with the addition of the following: dotted line, calculated IAM-SCAR data of Maljković *et al*. [20]; solid circles, experimental data of Maljković *et al*. [20].

and IAM-SCAR of Palihawadana *et al*. [19], and the *R*-matrix DCS of Mašín *et al*. [23] in the CC framework are also shown for comparison. At 3 and 6 eV, our dipole-corrected DCS still retain some oscillations. This behavior was also observed for other polar targets such as methanol and ethanol [40,49] and could possibly be a limitation of the point-dipole Born-correction procedure. However, the calculated DCS becomes smoother with increasing incident energies. Quantitatively, since the measured data of Palihawadana *et al*. [19] started at 20°, our theoretical results both with and without the Born correction are in fairly good agreement with their measured data. In this energy range, the theoretical DCS calculated using the SMC are in generally good agreement with our Born-corrected data, except at scattering angles near the forward direction. Again, the lack of the Born-dipole correction in their data is the origin of this discrepancy. The comparison of our data with the CC DCS of Mašín *et al*. [23] also shows reasonably good agreement. As expected, the IAM-SCAR data at 6 and 10 eV strongly disagree with all the theoretical results, as well as with the experimental data.

In Figs. 9 and 10, we present the theoretical results of Born-dipole-corrected DCS in the 20–300 eV energy range. In this range, our calculations were performed including absorption effects via the SQFSM approach. The experimental results of Palihawadana *et al*. [19] up to 50 eV and those of Maljković *et al*. [20] in the 50–300 eV range along with the theoretical data calculated using the SMC [19] and IAM-SCAR [19,20] are also shown for comparison. At 20 eV, our calculated data are still in good agreement with the SMC DCS obtained at the SEP level of approximation, which indicates

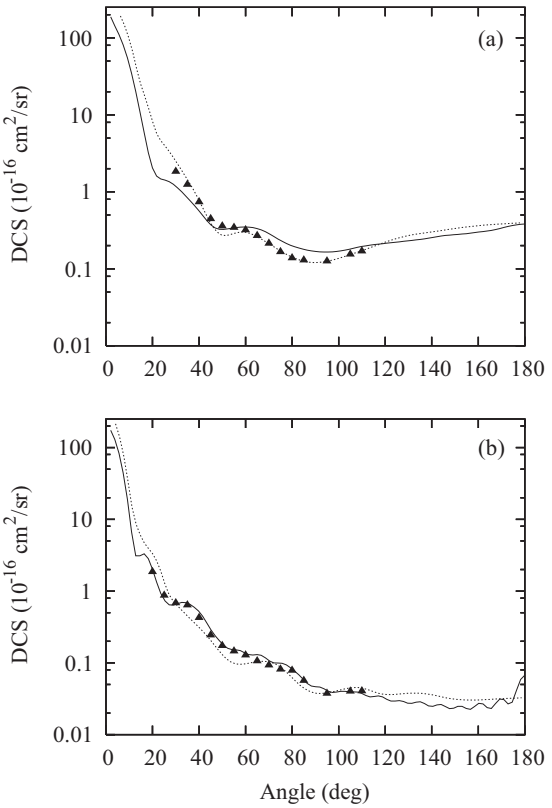

FIG. 10. DCS for elastic e^--$C_4H_4N_2$ scattering at (a) 100 eV and (b) 300 eV. Symbols are the same as those in Fig. 9.

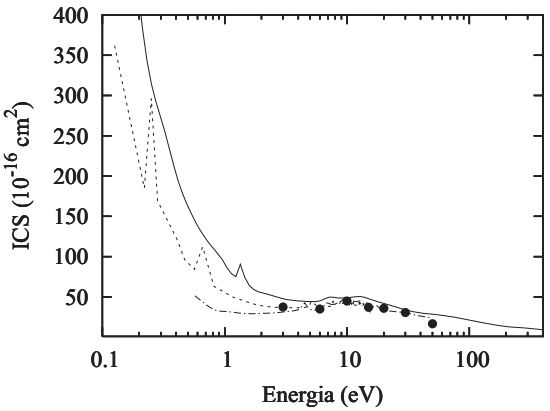

FIG. 11. ICS for elastic e^--$C_4H_4N_2$ scattering. Solid line, present theoretical results; short-dashed line, calculated CC data of Mašín *et al*. [23]; dotted-dashed line, calculated SMC data of Palihawadana *et al*. [19]; solid circles, experimental data of Palihawadana *et al*. [19]. All the calculations were performed without the Born-dipole correction.

that absorption is not yet significant even for this larger target. Again, the IAM-SCAR DCS are significantly different from our data. The comparison of our DCS with the experimental data shows a good qualitative agreement. Quantitatively, good agreement is also seen at angles up to 40°. Above this angle, our calculation overestimates the measured data. At 50 eV, the SMC DCS calculated without accounting for absorption effects lie significantly above our data at intermediate and large scattering angles, which clearly indicates the significant influence of such effects. At this energy, there is a reasonably good agreement between our calculated results and the two sets of experimental data [19,20]. Also, there is a significant improvement in the agreement between the IAM-SCAR data and our data. In the 100–300 eV range, there is a generally good agreement between our calculated results and the experimental and IAM-SCAR data of Maljković *et al*. [20].

In Fig. 11 we show our ICS calculated without the Born-dipole correction for elastic e^--$C_4H_4N_2$, in comparison with the corresponding data obtained by SMC [19] and by the *R*-matrix method at the SEP level of approximation [23]. The experimental results of Palihawadana *et al*. [19] in the 3–50 eV energy range are also presented. At energies above 3 eV, there is a good agreement among the calculated data and the experimental ICS. However, at energies near threshold, the three sets of theoretical ICS are different from each other, with our calculated data lying well above the others. Moreover, the ICS of Mašín *et al*. [23] calculated at the SEP level of approximation show two very sharp resonances centered at 0.21 eV ($^2A_2$) and 0.63 eV ($^2B_1$), respectively, and one broad resonance located at 5.15 eV ($^2B_1$). These resonances were also identified by Winstead and McKoy [50] but in a different order, namely, $^2B_1$, $^2A_2$, and $^2B_1$. In our calculation we have identified one sharp resonance located at 1.4 eV and another broad resonance located at about 7.5 eV. The partial-channel analysis of our ICS showed that both resonances are of $^2B_1$ symmetry and are probably the same as those identified by Mašín *et al*. [23], but shifted to higher incident energies, probably due to the different treatment of the polarization effects.

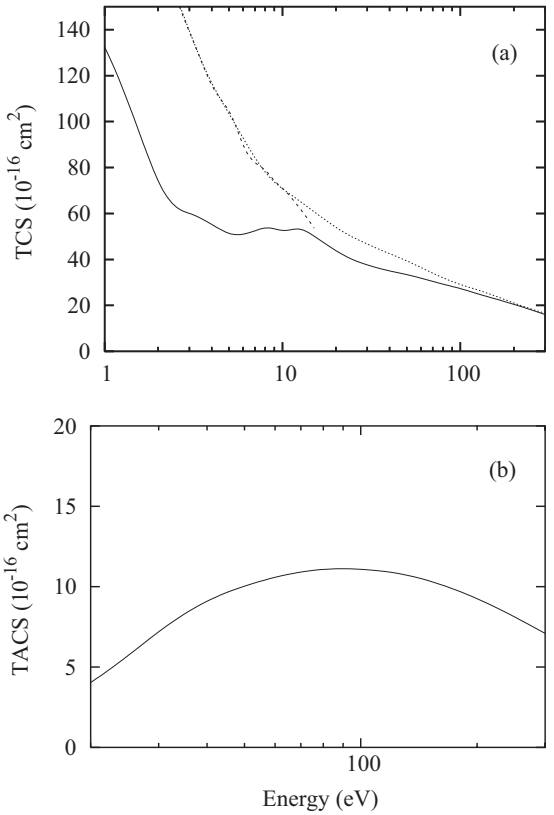

FIG. 12. (a) TCS and (b) TACS for e^--$C_4H_4N_2$ scattering. Solid line, present theoretical results calculated including absorption effects; short-dashed line, calculated SEP results of Mašín *et al*. [23] with the Born-dipole correction; dotted line, calculated IAM-SCAR data of Zecca *et al*. [24].

In Fig. 12(a) we present our TCS calculated with the Born-dipole correction at incident energies up to 300 eV. The ICS calculated with the *R*-matrix method with the SEP + Born-dipole correction [23] and the TCS obtained using the SCAR + rotational excitation of Zecca *et al*. [24] are also shown for comparison. Unfortunately, there are no reported experimental TCS in the literature. At low energies, both the *R*-matrix ICS and SCAR TCS lie well above our results. This discrepancy is probably due to the different ways of performing the dipole correction. In our calculation, this correction is made on the scattering amplitudes, whereas in SCAR and *R*-matrix calculations it is made directly on the cross sections. However, there is a good agreement between the SCAR TCS and our results for energies above 50 eV. In Fig. 12(b), we present our calculated results for TACS. Unfortunately, there are no experimental or calculated data to compare with.

IV. CONCLUDING REMARKS

In the present work, we report a theoretical study on e^--CH_2O and e^--$C_4H_4N_2$ scatterings in the low- and intermediate-energy ranges. These targets are both strongly polar. Due to this characteristic, DCS at near the forward direction are sharply peaked. Also, the ICS and TCS at very low incident energies are strongly enhanced. Our method was able to provide DCS in reasonably good agreement with

other theoretical results and experimental data available in the literature. Particularly for CH_2O, our calculations were able to predict a $^2B_1$ shape resonance located at around 1.0 eV, in agreement with previous calculations [10,15,16]. Experimental evidence of this resonance was observed by Benoit and Abouaf [8]. Also for $C_4H_4N_2$, our calculations have identified two $^2B_1$ shape resonances located at about 1.4 and 7.5 eV, respectively. These resonances are probably the same as those observed by Mašín *et al*. [23], although slightly shifted to higher incident energies. Nevertheless, the $^2A_2$ shape resonance identified by them located at 0.21 eV was not observed in the present study. Different ways to compute the correlation-polarization potential may be the reason for this discrepancy.

At energies above 30 eV, absorption effects become relevant. Therefore, the DCS calculated accounting for such effects lie below those obtained without them, particularly at intermediate and large scattering angles. In general, DCS and ICS including absorption effects are in better agreement with the experimental data available in the literature. Due to the lack of experimental and/or theoretical studies for e^--CH_2O scattering, mainly in the intermediate-energy region, we hope that the present study may stimulate further investigation on this target.

ACKNOWLEDGMENTS

This research was partially supported by the Brazilian agencies CNPq and FAPESP.

[1] R. K. Janev, in *Atomic and Plasma-Material Interaction Processes in Controlled Thermonuclear Fusion*, edited by R. K. Janev and H. W. Drawin (Elsevier, Amsterdam, 1993), p. 27.
[2] J. J. Perry, Y. H. Kim, J. L. Fox, and H. S. Porter, J. Geophys. Res. **104**, 16541 (1999).
[3] W. L. Morgan, Adv. At. Mol. Opt. Phys. **43**, 79 (2000).
[4] B. Boudaiffa, P. Cloutier, D. Hunting, M. A. Huels, and L. Sanche, Science **287**, 1658 (2000).
[5] M. J. Weiss, C. E. Kuyatt, and S. Mielczarek, J. Chem. Phys. **54**, 4147 (1971).
[6] A. Chutjian, J. Chem. Phys. **61**, 4279 (1974).
[7] P. D. Burrow and J. A. Michejda, Chem. Phys. Lett. **42**, 223 (1976).
[8] C. Benoit and R. Abouaf, Chem. Phys. Lett. **123**, 134 (1986).
[9] E. H. Van Veen, W. L. Van Dijk, and H. H. Brongersma, Chem. Phys. **16**, 337 (1976).
[10] T. N. Rescigno, C. W. McCurdy, and B. I. Schneider, Phys. Rev. Lett. **63**, 248 (1989).
[11] T. N. Rescigno, B. H. Lengsfield, and C. W. McCurdy, Phys. Rev. A **41**, 2462 (1990).
[12] B. I. Schneider, T. N. Rescigno, and C. W. McCurdy, Phys. Rev. A **42**, 3132 (1990).
[13] S. Mahalakshmi and M. K. Mishra, Chem. Phys. Lett. **296**, 43 (1998).
[14] A. A. Sobrinho, L. E. Machado, S. E. Michelin, M.-T. Lee, and L. M. Brescansin, J. Mol. Struct. (THEOCHEM) **539**, 65 (2001).
[15] S. Kaur and K. L. Baluja, J. Phys. B **38**, 3917 (2005).
[16] T. C. Freitas, M. A. P. Lima, S. Canuto, and M. H. F. Bettega, Phys. Rev. A **80**, 062710 (2009).
[17] A. Zecca, E. Trainotti, L. Chiari, G. García, F. Blanco, M. H. F. Bettega, M. T. do N. Varella, M. A. P. Lima, and M. J. Brunger, J. Phys. B **44**, 195202 (2011).
[18] M. Vinodkumar, H. Bhutadia, B. Antony, and N. Mason, Phys. Rev. A **84**, 052701 (2011).
[19] P. Palihawadana, J. Sullivan, M. Brunger, C. Winstead, V. McKoy, G. Garcia, F. Blanco, and S. Buckman, Phys. Rev. A **84**, 062702 (2011).
[20] J. B. Maljković, A. R. Milosavljević, F. Blanco, D. Šević, G. García, and B. P. Marinković, Phys. Rev. A **79**, 052706 (2009).
[21] P. L. Levesque, M. Michaud, and L. Sanche, J. Chem. Phys. **122**, 094701 (2005).
[22] D. B. Jones, S. M. Bellm, P. Limão-Vieira, and M. J. Brunger, Chem. Phys. Lett. **535**, 30 (2012).
[23] Z. Mašín, J. D. Gorfinkiel, D. B. Jones, S. M. Bellm, and M. J. Brunger, J. Chem. Phys. **136**, 144310 (2012).
[24] A. Zecca, L. Chiari, G. García, F. Blanco, E. Trainotti, and M. J. Brunger, J. Phys. B **43**, 215204 (2010).
[25] G. Staszewska, D. W. Schwenke, and D. G. Truhlar, Phys. Rev. A **29**, 3078 (1984).
[26] F. Blanco and G. García, Phys. Lett. A **255**, 147 (1999).
[27] G. Staszewska, D. W. Schwenke, D. Thirumalai, and D. G. Truhlar, Phys. Rev. A **28**, 2740 (1983).
[28] M.-T. Lee, I. Iga, L. E. Machado, L. M. Brescansin, E. A. y Castro, I. P. Sanches, and G. L. C. de Souza, J. Electron Spectrosc. Relat. Phenom. **155**, 14 (2007).
[29] E. A. y Castro, G. L. C. de Souza, I. Iga, L. E. Machado, L. M. Brescansin, and M.-T. Lee, J. Electron Spectrosc. Relat. Phenom. **159**, 30 (2007); **159**, 012709 (2010).
[30] P. Rawat, M. G. P. Homem, R. T. Sugohara, I. P. Sanches, I. Iga, G. L. C. de Souza, A. S. dos Santos, R. R. Lucchese, L. E. Machado, L. M. Brescansin, and M.-T. Lee, J. Phys. B **43**, 225202 (2010).
[31] G. L. C. de Souza, M.-T. Lee, I. P. Sanches, P. Rawat, I. Iga, A. S. dos Santos, L. E. Machado, R. T. Sugohara, L. M. Brescansin, M. G. P. Homem, and R. R. Lucchese, Phys. Rev. A **82**, 012709 (2010).
[32] G. Staszewska, P. Staszewski, and K. Zebrowski, J. Electron Spectrosc. Rel. Phenom. **168**, 40 (2008).
[33] N. T. Padial and D. W. Norcross, Phys. Rev. A **29**, 1742 (1984).
[34] S. Hara, J. Phys. Soc. Jpn. **22**, 710 (1967).
[35] R. R. Lucchese and V. McKoy, Phys. Rev. A **28**, 1382 (1983).
[36] F. A. Gianturco, R. R. Lucchese, and N. Sanna, J. Chem. Phys. **102**, 5743 (1995).
[37] P. G. Burke, N. Chandra, and F. A. Gianturco, J. Phys. B **5**, 2212 (1972).
[38] L. E. Machado, L. M. Brescansin, I. Iga, and M.-T. Lee, Eur. Phys. J. D **33**, 193 (2005).
[39] L. M. Brescansin, L. E. Machado, M.-T. Lee, H. Cho, and Y. S. Park, J. Phys. B **41**, 185201 (2008).
[40] M.-T. Lee, G. L. C. de Souza, L. E. Machado, L. M. Brescansin, A. S. dos Santos, R. R. Lucchese, R. T. Sugohara, M. G. P. Homem, I. P. Sanches, and I. Iga, J. Chem. Phys. **136**, 114311 (2012).

[41] M. E. Rose *Elementary Theory of Angular Momentum* (Wiley, New York, 1957).
[42] T. H. Dunning, Jr., J. Chem. Phys **53**, 2823 (1970).
[43] J. N. Shoolery and A. H. Sharbaugh, Phys. Rev. **82**, 95 (1951).
[44] R. R. Lucchese, G. Raseev, and V. McKoy, Phys. Rev. A **25**, 2572 (1982).
[45] Y.-K. Kim and K. K. Irikura, in *Proceedings of the Second International Conference on Atomic and Molecular Data and Their Applications*, edited by K. A. Berrington and K. L. Bell, AIP Conference Proceedings, Vol. 53 (AIP, New York, NY, 2000), p. 220. Data available at http://physics.nist.gov/PhysRefData/Ionization.
[46] M. W. Schmidt *et al*., J. Comput. Chem. **14**, 1347 (1993).
[47] http://cccbdb.nist.gov.
[48] G. L. Blackman, R. D. Brown, and F. R. Burden, J. Mol. Spectrosc. **35**, 444 (1970).
[49] M. A. Khakoo, J. Blumer, K. Keane, C. Campbell, H. Silva, M. C. A. Lopes, C. Winstead, V. McKoy, R. F. da Costa, L. G. Ferreira, M. A. P. Lima, and M. H. F. Bettega, Phys. Rev. A **77**, 042705 (2008).
[50] C. Winstead and V. McKoy, J. Chem. Phys. **125**, 174304 (2006).